

Type Ia supernovae and stellar winds in AGN driven relativistic bubbles

N. N. Chugai^{1,2*}, E. M. Churazov^{1,3}, R. A. Sunyaev^{1,3}

¹Max-Planck-Institut für Astrophysik, Karl-Schwarzschild-Str. 1, D-85741 Garching, Germany

²Institute of Astronomy of Russian Academy of Sciences, Pyatnitskaya St. 48, 109017 Moscow, Russia

³Space Research Institute, Profsoyuznaya 84/32, Moscow 117810, Russia

28 January 2011

ABSTRACT

We analyse behavior of stellar winds of evolved stars and the outcome of SN Ia explosions in the AGN driven relativistic bubble. We find that the expansion of wind shells is efficiently decelerated by the relativistic pressure; their bulk motion however is preserved so they cross the bubble together with the parent star. The wind material occupies a small fraction of bubble volume and does not affect substantially the expansion of SN remnants. The estimated maximal radius of a SN remnant in the bubble is 30–40 pc, if the envelope keeps its integrity and remains spherical. A fragmentation of SN shell due to Rayleigh-Taylor instability can alleviate the propagation of the SN material so the ejecta fragments are able to cross the relativistic bubble. Outside the bubble wind shells and supernova fragments are decelerated in the intracluster medium at close range off the bubble boundary. The deposited SNe Ia material can enrich the intracluster gas with metals in a thin layer at the boundary of the relativistic bubble. This process may lead to a rim of enhanced line emission. In the opposite limit, when the fragmentation of supernova remnant is moderate or absent, the SN Ia matter is advected by the relativistic plasma and may leave the central region of the bright cluster galaxy together with buoyantly moving bubbles.

Key words: galaxies: clusters.

1 INTRODUCTION

Radio and X-ray observations show that in majority of regular galaxy clusters, possessing a cool core, the activity of a central supermassive black hole mediated by AGN jets creates bubbles of relativistic plasma in the intra-cluster medium (ICM) (Böhringer et al. 1993; Huang & Sarazin 1998; Churazov et al. 2000; McNamara et al. 2000; Birzan et al. 2004). X-ray data are consistent with the assumption that bubbles are completely devoid of thermal gas (Sanders & Fabian 2007) although the limits on the amount of thermal gas in the bubbles are not very tight. The absence of strong shocks in the ICM surrounding the bubbles implies that the relativistic plasma is in approximate pressure equilibrium with the ICM. These bubbles, inflated by an AGN, are believed to be responsible for mechanical coupling of the AGN energy release and the thermal state of the ICM in galaxy clusters, groups and individual elliptical galaxies. For this reason every aspect of bubble physics receives much attention.

Given the ubiquity of bubbles in clusters, these objects should be almost always present in the cluster core. The lifetime of the bubble in the stratified atmosphere is set by “buoyancy” time, while

the growth rate of the bubble is defined by the power of the AGN (e.g., Gull & Northover 1973; Churazov et al. 2000). Pairs of bubbles are located on both sides of the central supermassive black hole and often several generation of bubbles differing in their size and the distance from the center are observed.

Bubbles with sizes of order 1–10 kpc are often found in the inner regions of galaxy clusters, sharing the space with brightest cluster galaxy (BCG). For example, in NGC 1275 (BCG of Perseus cluster) within the effective radius of the galaxy ($R_e \sim 15$ kpc) we see two bubbles on either side of the nucleus with the radius of each bubble ~ 6.3 kpc (e.g., Böhringer et al. 1993; Fabian et al. 2003). In M 87 (Virgo cluster) the bubble radius is ~ 1.4 kpc (e.g., Forman et al. 2005, 2007), while the galaxy effective radius is of order 7.7 kpc. We expect that in both cases bubbles should contain significant fraction of the galaxy stars. These old low mass stars evolve as usual, lose their mass via the wind, and some of them give birth to type Ia supernovae (SNe Ia). Even if the relativistic bubble sweeps up all the thermal gas in the process of inflation a lot of material in the form of the stellar wind thus can be supplied by the stars *inside the bubble* during the bubble life. This wind material could affect the expansion dynamics of supernovae exploded in the bubble.

The question we address here is what happens to the stellar

* E-mail: nchugai@inasan.ru

winds and SNIa ejecta embedded in the relativistic bubble. Almost weightless relativistic plasma provides highly unusual conditions for the dynamic evolution of wind shells and SNe. Two extreme scenarios are conceivable. In one limit all the wind material and SN ejecta are decelerated and mixed with relativistic plasma. During subsequent evolution the buoyantly rising bubbles advect this material with them. In another limit the matter ejected by evolving stars propagates freely through the relativistic plasma, attains the boundaries of the bubble and enriches the ICM just outside the bubble with heavy elements. We investigate different scenarios of dynamical evolution of wind shells and SN ejecta and explore observational outcomes of these scenarios.

The structure of the paper is as follows. We first study the expansion and bulk motion of the wind envelopes including mass stripping effects. This provides us with the estimate of the filling factor of the wind shells ensemble. We then address the issue of the SN envelope expansion dynamics and bulk motion, Rayleigh-Taylor fragmentation of the SN shell and propagation of ejecta fragments in the relativistic plasma. Finally, we discuss the implications of results for the relativistic bubble matter contents and intracluster thermal environment.

2 WIND MATERIAL IN RELATIVISTIC BUBBLE

2.1 Stars and mass injection rate

We consider, as a fiducial model, a spherical bubble of radius $R_b = 5$ kpc with the bubble center at the distance R_b from the center of the BCG. The characteristic age of this bubble is $t_b \sim 2R_b/v_b \sim 3.3 \times 10^7$ yr, where we adopt the bubble rise velocity $v_b = 300$ km s⁻¹ (cf. Churazov et al. 2001). At the radii $r < 15$ kpc the stellar component in massive elliptical galaxies dominates (e.g. Johnson et al. 2009) and its density distribution can be approximated by the singular isothermal sphere with the velocity dispersion σ_v

$$\rho = \frac{\sigma_v^2}{2\pi G r^2} = \rho_0 \left(\frac{r_0}{r} \right)^2, \quad (1)$$

where G is gravitational constant and r_0 is a radial scale¹. Adopting $r_0 = 10$ kpc and velocity dispersion $\sigma_v = 350$ km s⁻¹ (Wu & Tremaine 2006) one gets the stellar mass $M(< r_0) = M_0 = 5.6 \times 10^{11} M_\odot$. This value is consistent with estimates of the total mass of stellar component of BCG of $\sim 10^{12} M_\odot$. Inside the bubble of radius $R_b = 5$ kpc the stellar mass in this case is $M_s \approx 9 \times 10^{10} R_{b,5} M_\odot$, where $R_{b,5} = R_b/(5 \text{ kpc})$.

The stars are presumably old with an age of $t \sim 10^{10}$ yr, which suggests that the current upper limit of the stellar mass at the AGB stage is $\approx 1 M_\odot$ (Schaller et al. 1992). Assuming the Salpeter initial mass function $dN/dm = C m^{-\alpha}$ within the range $m_1 < m < m_2$ one gets the normalizing factor

$$C = (\alpha - 2) M_s [m_1^{-(\alpha-2)} - m_2^{-(\alpha-2)}]^{-1} = 0.28 M_s, \quad (2)$$

where $\alpha = 2.35$, $m_1 = 0.1 M_\odot$, and $m_2 = 1 M_\odot$ are used.

The star of $m = 1 M_\odot$ leaves behind a white dwarf of $m_{wd} = 0.5 M_\odot$ (Salaris et al. 2009), while $\Delta m = m - m_{wd} = 0.5 M_\odot$ is lost in the form of slow ($u \approx 10 - 30$ km s⁻¹) wind during the thermally pulsing AGB stage (Vassiliadis & Wood 1993). The present day integrated rate of the wind matter injection into the relativistic bubble is

$$\dot{M} = (m_2 - m_{wd}) \frac{dN}{dm} \frac{dm_2}{dt}, \quad (3)$$

where dm_2/dt is the rate at which upper limit m_2 decreases with time. This rate is determined by the relation between the lifetime and initial star mass $t = t_2(m_2/m)^\beta$, where $\beta = 3.2$ in the range of $1 - 2 M_\odot$ (Schaller et al. 1992). For these values and $M_s = 9 \times 10^{10} R_{b,5} M_\odot$ the equation (3) yields $\dot{M} = 0.416 M_\odot R_{b,5} \text{ yr}^{-1}$. The corresponding stellar death rate is $\dot{N} = 0.83 R_{b,5} \text{ yr}^{-1}$ which is also the rate of wind shell formation \dot{N}_w . One expect thus to find $N_w = t_b \dot{N}_w \approx 2.7 \times 10^7 R_{b,5}$ newly created wind envelopes in the bubble volume with the total amount of the wind matter in the bubble of $0.5 N_w \approx 1.4 \times 10^7 R_{b,5} M_\odot$, factor $\sim 10^4$ larger than the mass in the form of relativistic particles of the bubble, $3pV/c^2 \sim 2.4 \times 10^3 M_\odot$. It should be noted, however, that the N_w estimate ignores so far a possible escape of wind envelopes from the bubble, which is addressed below.

2.2 Wind shell dynamics

The dynamical effect of the wind matter in the bubble on a certain wind shell or SN ejecta depends on the filling and covering factors of wind shells. To assess the situation one needs first to find the average volume and size of a wind envelope at the final stage of its expansion. Here we assume that the bubble is static and adopt that a star moves with the mean velocity v_s . Despite a singular isothermal sphere is assumed for the stellar population, it is reasonable to estimate v_s using Maxwell velocity distribution truncated at the escape velocity v_e . The truncated Maxwell distribution is taken in the form proposed by (King 1966): $f(v) \propto [\exp(-v^2/2\sigma_v^2) - \exp(-v_e^2/2\sigma_v^2)]$ for $v < v_e$ and $f = 0$ otherwise. Adopting $\sigma_v = 350$ km s⁻¹, i.e., $v_e = 2\sigma_v = 700$ km s⁻¹ we come to the average velocity $v_s = 400$ km s⁻¹.

The geometry of the wind shell that forms as a result of the interaction of the wind with the relativistic medium depends on the value of the drag force exerted on the wind boundary. If the drag force is strong the stripped wind material creates a trailing plume. On the other hand, if drag force is very weak, then the wind shell moves with the star velocity retaining spherically-symmetric shape and eventually may escape the relativistic bubble. To explore this issue we consider major stages of the mass loss at the AGB and post-AGB stage: (Steffen et al. 1998; Lou et al. 2010): (1) the slow wind ($u = 10$ km s⁻¹, $\dot{M} \sim 10^{-7} M_\odot \text{ yr}^{-1}$) on the time scale of the AGB stage, i.e., 10^6 yr, (2) slow superwind ($\dot{M} \sim 10^{-5} - 10^{-4} M_\odot \text{ yr}^{-1}$) during the last $\sim 10^4$ yr of the AGB stage, and (3) fast wind at the post-AGB stage which corresponds to the planetary nebula (PN) stage ($\sim 10^4$ yr). The last stage practically does not contribute to the mass loss, but turns out essential for the acceleration of the slow wind. We adopt that 60% of the hydrogen shell is lost at the first stage and 40% at the superwind stage (Steffen et al. 1998), which implies the mass-loss rates $\dot{M} \sim 3 \times 10^{-7} M_\odot \text{ yr}^{-1}$ at the slow wind stage and $\dot{M} \sim 2 \times 10^{-5} M_\odot \text{ yr}^{-1}$ at the superwind stage. For the fast wind stage we adopt parameters derived from the modelling of the X-ray emission of the PN: $\dot{M} \sim 2 \times 10^{-8} M_\odot \text{ yr}^{-1}$ and $u = 1500$ km s⁻¹ (Lou et al. 2010). The fast wind parameters suggest that the total kinetic energy released during this stage ($\sim 10^4$ yr) is $E_3 \approx 4.5 \times 10^{45}$ erg. When transferred to the slow wind shell with the mass of $0.5 M_\odot$ this energy accelerates the shell up to $u \approx 30$ km s⁻¹, in accord with the expansion velocities of evolved PN (Richer et al. 2008).

The mass stripping rate of the wind shell scales as the shell radius squared, so at the stage of slow wind the maximal stripping is attained at the end of this stage. The radius of the wind shell at

¹ This approximation breaks at large radii to ensure convergence of the total stellar mass.

this age can be estimated from the energy arguments. The kinetic energy of the wind shell is spent on the pV work against external pressure p and on the internal energy which results in the stopping radius of the wind shell

$$r_1 = \left[\frac{3}{8\pi} \left(\frac{\gamma - 1}{\gamma} \right) \frac{M_1 u_1^2}{p} \right]^{1/3} = 0.19 p_{10}^{-1/3} \text{ pc}, \quad (4)$$

where $p_{10} = p/(10^{-10} \text{ erg cm}^{-3})$, $\gamma = 5/3$, $u_1 = 10 \text{ km s}^{-1}$, and $M_1 = 0.3 M_\odot$ are used.

The wind shell moves as a whole together with the white dwarf unless the bulk of the material is stripped into the trailing plume. The wind shell stripping can be estimated following Nulsen (1982) consideration of the gas stripping for a galaxy moving in the ICM. The turbulent stripping is determined by the combined effect of the Kelvin-Helmholtz instability (KHI) and the ram pressure drag. Indeed, KHI broadens the boundary layer which results in the suppression of the KHI. The net stripping rate, therefore, is controlled by the ram pressure

$$\dot{M} = \pi r_1^2 \rho_a v_s = 1.6 \times 10^{-12} p_{10}^{1/3} M_\odot \text{ yr}^{-1}, \quad (5)$$

where we use $\rho_a = 3p/c^2$ for the density of ambient medium. The average residence time of a wind shell in the bubble is $R_b/v_s \sim 1.2 \times 10^7 \text{ yr}$, so the above mass loss rate implies that the wind shell loses $\sim 2 \times 10^{-5} M_\odot$ while moving in the bubble, negligibly small amount compared to the mass of the wind shell, $0.3 M_\odot$.

Alternatively, the stripping could be caused by the Alfven wave drag. In this regard we note that the infinite conductivity approximation for the wind shell is fully applicable. A conducting body moving with velocity v across the magnetic field B experiences the drag force due to Alfven wave generation (Drell et al. 1965)

$$F_d = (B^2/4\pi)(v/v_A)S, \quad (6)$$

where S is the area of lateral surface perpendicular to \vec{B} , v_A is the Alfven velocity, $v_A \approx B/\sqrt{4\pi\rho_a}$ with $\rho_a = 3p/c^2$. Strictly speaking, the Alfven velocity in the relativistic plasma (Gedalin 1993) is smaller compared to this expression by a factor of 0.7-0.9 depending on the ratio of magnetic to total pressure; we neglect this difference. For a sphere of the radius r the lateral area is $S \approx 2\pi r^2$ and the mass stripping rate caused by the Alfven wave drag is

$$\dot{M} = \frac{B^2 r_w^2}{2v_A} \approx 4.1 \times 10^{-10} p_{10}^{7/6} B_5 M_\odot \text{ yr}^{-1}, \quad (7)$$

where $B_5 = B/(10^{-5} \text{ G})$. The stripping rate due to the Alfven drag thus turns out two orders of magnitude larger than the rate according to equation (5). Yet even for the Alfven drag the mass lost during the residence time is only $\sim 0.01 M_\odot$ which is a small fraction ($\sim 3\%$) of the wind shell. We thus conclude that the wind shell lost at the slow wind stage remains almost intact while traveling across the bubble. A similar result can be obtained for the superwind stage. The outcome of a combined effect of all three stages of the mass loss is a spherical wind shell of $0.5 M_\odot$ expanding with the velocity of 30 km s^{-1} . Using equation (4) one finds the wind shell stopping radius is $r_w = 0.5 p_{10}^{-1/3} \text{ pc}$.

The above treatment of the wind dynamics suggests that the cosmic rays diffusion into the shell can be neglected. To check whether this assumption is valid we assume Bohm diffusion coefficient $r_g c/3$, where r_g is the proton gyroradius. This assumption is standard for the analysis of cosmic ray propagation and supported by observational data on the cosmic ray acceleration in supernova remnants (Stage et al. 2006), although the concept of a tangled field might seriously modify a picture of the cosmic ray diffusion in

magnetic field (Narayan & Medvedev 2001). For the spectral index of relativistic protons > 2 the energy of cosmic rays resides in low energy protons, which permits us to use the characteristic energy of relativistic protons $\sim 1 \text{ GeV}$. With $B = 10^{-5} \text{ G}$ one gets $r_g \sim 3 \times 10^{11} \text{ cm}$. The diffusion time is then

$$t_d \sim \frac{r_w^2}{r_g c} = 3 \times 10^6 B_5^{-1} r_{w,18}^2 \text{ yr}, \quad (8)$$

where $r_{w,18} = r_w/(10^{18} \text{ cm})$. For the slow wind stage with the final radius of $r_1 \sim 0.2 \text{ pc}$ the diffusion time is comparable to the duration of this stage ($\sim 10^6 \text{ yr}$), while the life time of superwind and fast wind stages is significantly smaller than the diffusion time.

The estimated time scale of the cosmic ray diffusion suggests that the penetration of cosmic rays in the wind can affect the wind expansion dynamics at the slow wind stage making the pressure gradient smoother and the deceleration less pronounced. As a result, the final radius of the wind shell at the slow wind stage in fact could be somewhat larger, $r_1 > 0.2 \text{ pc}$. On the other hand, the effect cannot be significant because the diffusion time increases $\propto r_1^2$, so the role of the cosmic ray diffusion rapidly drops for larger radius. We conclude therefore that the stopping radius of the wind shell ($r_w \sim 0.5 \text{ pc}$), which includes the combined effect of AGB and post AGB mass loss and omits the cosmic ray diffusion, is a reasonable estimate.

2.3 Wind shell escape

Outside the relativistic bubble the wind shell turns out in the intracluster thermal gas. For the mass stripping rate $\dot{M} = \pi r_w^2 \rho_a v_s$ adopting the wind shell radius $r_w = 1.5 \times 10^{18} \text{ cm}$, number density of interstellar gas $n = 0.02 \text{ cm}^{-3}$, and $v_s = 400 \text{ km s}^{-1}$ one obtains $\dot{M} \sim 1.7 \times 10^{-7} M_\odot \text{ yr}^{-1}$. It takes $3 \times 10^6 \text{ yr}$ to completely strip the $0.5 M_\odot$ wind shell over the distance of $\sim 1 \text{ kpc}$. The same estimate can be obtained from the equation of deceleration of the wind shell as a whole by drag force $\pi r_w^2 \rho_a v_s^2$. The wind shell escaping bubble is decelerated thus in a close vicinity of the bubble boundary.

The average residence time of the wind shell in the bubble $R_b/v_s \sim 1.2 \times 10^7 \text{ yr}$ is somewhat smaller than the age of the fiducial bubble $3 \times 10^7 \text{ yr}$. The total amount of the wind shells residing in the bubble is, therefore, $\dot{N} R_b/v_s \sim 10^7$, while the filling factor of the ensemble of wind shells in the bubble is

$$f = N_w (R_w/R_b)^3 \sim 10^{-5} p_{10}^{-1}. \quad (9)$$

The probability of a collision with the wind shell is determined by the ratio of the bubble radius and the mean free path. The latter is

$$\lambda = (\pi r_w^2 n_w)^{-1} = 64 p_{10}^{2/3} \text{ kpc} \quad (10)$$

where $n_w = (3/4\pi) N_w/R_b^3 = 2 \times 10^{-5} \text{ pc}^{-3}$ is the number density of wind shells. The probability of shell collisions is low, because the average number of wind shells along the bubble radius is only $\tau = R_b/\lambda = 0.08$. The average probability of the collision is approximately $\approx [1 - \exp(-\tau)] \approx \tau = 0.08$. More accurate estimate can be done using expression for the escape probability of the photon from a homogeneous sphere (Osterbrock 1989)

$$p_{\text{esc}} = \frac{3}{4\tau} \left[1 - \frac{1}{2\tau^2} + \left(\frac{1}{\tau} + \frac{1}{2\tau^2} \right) \exp(-2\tau) \right], \quad (11)$$

For $\tau = 0.08$ the equation (11) gives $p_{\text{esc}} = 0.94$. Most of wind shells therefore escape the bubble freely and only 6% of wind shells collide with another shell.

The fate of the collided wind shells depends on whether the

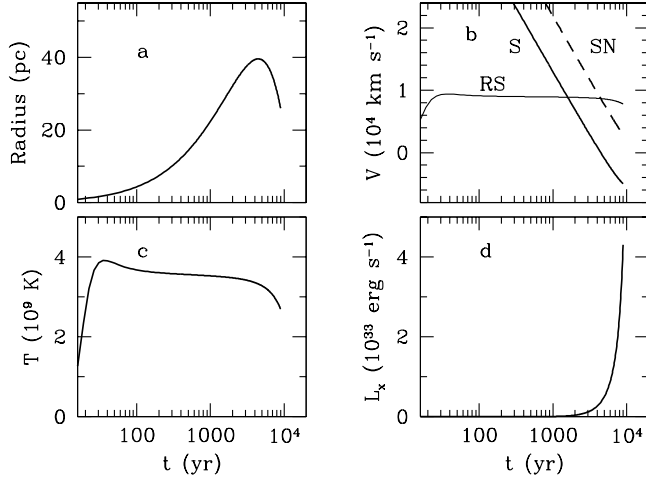


Figure 1. Thin shell model of supernova evolution in relativistic bubble. Shown are the shell radius (a), evolution of velocities of the shell (S), pre-shock velocity of supernova ejecta (SN), and reverse shock speed (RS) (b), evolution of the reverse shock temperature (c), X-ray luminosity (d).

collision is adiabatic or radiative. With the average relative velocity of collision $u \sim 560 \text{ km s}^{-1}$ and the wind shell density $\sim 200 \text{ cm}^{-3}$ the estimated cooling time of the shocked gas turns out to be $\sim 3 \times 10^{10} \text{ s}$, comparable with the hydrodynamic scale $r_w/u \sim 3 \times 10^{10} \text{ s}$. This means that both adiabatic and radiative collision regimes are plausible. In the adiabatic case wind shells approximately retain their sizes and absolute velocities, so the adiabatic collision does not affect their escape. In radiative case collided shells merge and form thin dense pancake of a thickness $b \ll r_w$ and density $\rho_c \sim (r_w/b)\rho_w$, where ρ_w is the density of the wind shell before collision. This pancake is liable to fragmentation into clumps of size $a \gtrsim b$ and average velocity $\sim v_s/\sqrt{2}$. It is easy to verify that for fragments with sizes $a \gtrsim b$ and density $\rho_c \sim (r_w/b)\rho_w$ the stripping (or deceleration) time is greater than the stripping time of wind shells. We thus conclude that the most of the wind material escapes into the hot ICM.

In our analysis of the wind shell dynamics we ignored a possible fragmentation of the wind shell due to the Rayleigh-Taylor (RT) instability on the deceleration or acceleration stages. This omission facilitates the consideration; yet it does not affect the major conclusion that the wind shell material escape the relativistic bubble. As we will see below, the RT fragmentation favours the shell matter escape.

3 TYPE IA SUPERNOVAE IN RELATIVISTIC BUBBLE

With SNIa production efficiency $\psi = 0.008$ per one white dwarf formed in the stellar population of E-galaxies (Pritchett et al. 2008) and the stellar death rate in the bubble of fiducial model $\dot{N} = 0.83 \text{ yr}^{-1}$ one expects $\psi \dot{N} t_b \sim 2 \times 10^5$ SNIa explosions during the relativistic bubble lifetime $t_b = 3 \times 10^7 \text{ yr}$. We now consider in detail SN expansion in the relativistic bubble and analyse an outcome of the Rayleigh-Taylor fragmentation of decelerating SN shell.

3.1 SN expansion

Given a small number of wind shells along the bubble radius (Section 2.3) the deceleration of the SN expansion in the relativistic bubble is probably dominated by the pressure of the relativistic

fluid. Indeed, for SN expanding with the characteristic velocity $v \approx (2E/M)^{1/2} = 10^9 \text{ cm s}^{-1}$ one readily sees that the ram pressure is small compared to the pressure of relativistic fluid: $\rho v^2 = 3p(v/c)^2 \ll p$. The crucial role of the external relativistic pressure in the SN deceleration is a distinguishing feature compared to the standard case of SN shell in the ordinary interstellar medium.

In our analysis of the SN expansion we assume the isotropic pressure of the relativistic medium. This is the case, if the mean free path for relativistic protons along the magnetic field is much less than the SN radius. Since the SN expands subsonically relative to the external medium, in which the sound speed is $\approx c/\sqrt{3}$, the strong forward shock does not form. The reverse shock obviously forms, because outer layers of ejecta are decelerated by the external pressure and the velocity jump between the undisturbed ejecta and swept-up shell exceeds the sound speed in the unshocked ejecta ($\sim 10 \text{ km s}^{-1}$). The SN is fully decelerated when the reverse shock crosses the bulk of the ejecta mass.

To estimate the stopping radius of SN one can use the energy considerations likewise we did for the wind shell expansion. The initial kinetic energy E of SN should be spent on the PV work against the external pressure and on the internal energy $pV/(\gamma - 1)$ which gives the stopping radius

$$r_{sn} = \left[\left(\frac{\gamma - 1}{\gamma} \right) \frac{3E}{4\pi p} \right]^{1/3} = 36 p_{10}^{-1/3} \text{ pc}. \quad (12)$$

With a characteristic ejecta velocity $v \approx 10^9 \text{ km s}^{-1}$ it takes $t_s \sim r_{sn}/v \sim 3 \times 10^3 \text{ yr}$ to reach r_{sn} , rather short time compared to the bubble lifetime.

The dynamics of the swept-up shell and the X-ray emission of the reverse shock can be illustrated using a model based on a thin shell approximation. This suggests that the shell formed by ejecta material flowing into the reverse shock is considered as a thin shell which dynamics is governed by the dynamical pressure of the SN ejecta and external pressure $p = 10^{-10} \text{ erg cm}^{-3}$. The equation of motion for the thin shell is

$$M \frac{dv}{dt} = 4\pi r^2 \left[\rho \left(\frac{r}{t} - v \right)^2 - p \right], \quad (13)$$

where the shell mass is determined by the mass conservation

$$\frac{dM}{dt} = 4\pi r^2 \rho \left(\frac{r}{t} - v \right). \quad (14)$$

These equations are solved numerically assuming a freely expanding SN with the mass of $1.4 M_\odot$, energy of $1.5 \times 10^{51} \text{ erg}$, the density distribution $\rho \propto \exp(-v/v_0)$, boundary velocity of $4 \times 10^4 \text{ km s}^{-1}$, and initial outer radius of 10^{18} cm .

Results are displayed in Fig. 1 which shows the evolution of the shell radius, velocity of the shell, boundary velocity of SN ejecta and velocity of the reverse shock, reverse shock temperature assuming full equilibration, and X-ray luminosity of the reverse shock. The maximal radius of the thin shell model is 39 pc, slightly larger than analytical estimate $r_{sn} = 36 \text{ pc}$. Remarkably, the thin shell shows contraction phase (Fig. 1a) which is a direct outcome of the dynamical role of the external pressure. However, since we neglect the internal pressure of the shocked envelope, the amplitude of the contraction phase in our model is exaggerated, so we stop the computations at this phase. To calculate the X-ray emission we assume that the hot plasma in the shell is distributed homogeneously in the shell with the thickness $\Delta R/R = 0.1$. It is rather a crude approximation because the density distribution in the reverse shock is expected to be essentially inhomogeneous with a peak at the con-

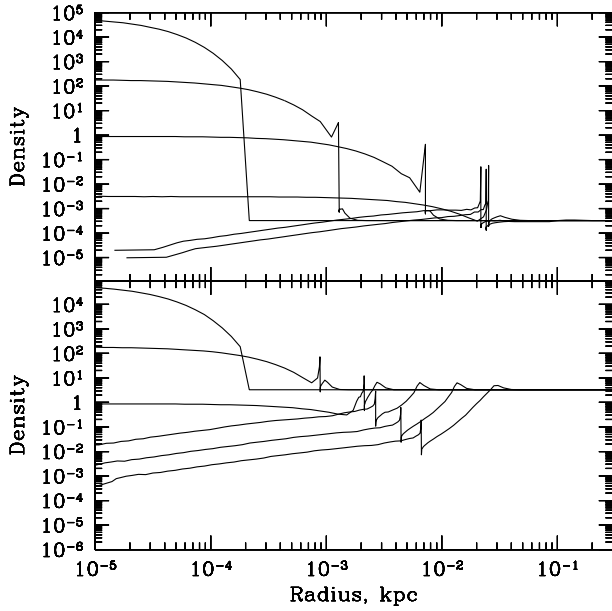


Figure 2. Density distribution for SNIa envelope expanding in the ICM at the ages $\sim 60, 400, 3000, 2 \times 10^4$ and 10^5 years for the ICM temperature of 0.01 keV (**bottom**) and of 100 keV (**top**). Position of a sharp wiggle in the density distribution corresponds to the contact discontinuity separating SN ejecta and the ICM.

tact surface. Yet it is reasonable enough to get an idea about X-ray luminosity within a factor of two. The luminosity is maximal at the contraction phase and reaches $\sim 4 \times 10^{33}$ erg s $^{-1}$ at the shock temperature of ~ 200 keV. The equilibration of electrons and ions, however, is an oversimplification, so the shock electron temperature and the luminosity should be considered approximate.

Another interesting view on the SN expansion dynamics in the relativistic bubble gives us one-dimensional hydrodynamic simulations in which we assume a hot rarefied non-relativistic plasma to be a proxy for the relativistic fluid. The thermal pressure is taken the same $p = 10^{-10}$ erg cm $^{-3}$. The ICM temperature varies in different runs from 10^{-2} up to 10^4 keV 2 . For $T = 10^4$ keV the situation is close to the case of the relativistic medium because the thermal pressure exceeds the dynamical pressure in the upstream flow of the forward shock. We assume homologous expansion of the envelope $v \propto r$ and model the initial density distribution 10 years after the explosion as $\rho \propto e^{-r/r_0}$, where $r_0 = 3 \times 10^{-5}$ pc. The ejecta mass is $1.4 M_\odot$ and kinetic energy is 1.5×10^{51} erg, while the maximum expansion velocity is set to 2×10^4 km s $^{-1}$.

The dependence of the expansion dynamics on the temperature of the ICM (at the same pressure) is apparent from Fig. 2. In the low temperature case (bottom panel in Fig. 2) most of ejecta energy is spent on a forward shock, which is barely resolved in our simple simulations. By contrast, for the high temperature ICM almost all the initial kinetic energy is eventually converted into the enthalpy of the ejecta and only tiny amount of energy is deposited in the forward shock. Accordingly the final size of the envelope at the boundary separating ejecta and ICM is much larger for the high temperature run. This is further illustrated in Fig. 3, showing the time dependence of the envelope radius. The simulations show that in the limit of very hot ICM the final envelope radius converges

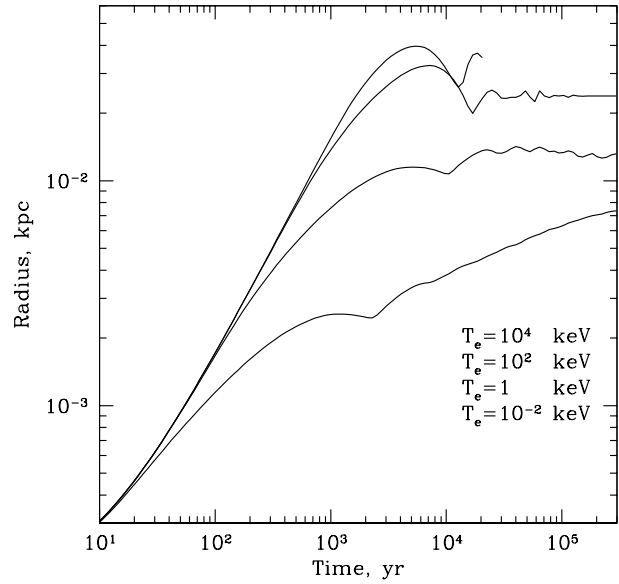


Figure 3. Radius of the contact discontinuity, separating SN ejecta and the ICM as a function of time. Four curves shown correspond to explosions in the ICM with the same pressure, but different temperatures, 0.01, 1, 100, 10^4 keV, from bottom to top. Clearly the final size of the ejecta is largest in the ICM with highest temperature.

to the value given by the thin shell model (Fig. 1). The X-ray luminosity of the reverse shock in the model with 10^4 keV medium is shown in Fig. 4 together with the evolution of the radii of the reverse shock and contact surface. The luminosity evolution is consistent with the prediction of the thin shell model (Fig. 1) at the ages $\lesssim 6 \times 10^3$ yr. However, at the final stage of the ejecta deceleration ($t \gtrsim 10^4$ yr) the luminosity behavior differs from that of the thin shell model. Indeed at this phase the shocked gas cannot be treated as thin shell. After about 10^4 yr the reverse shock attains the center. This is accompanied by the overall contraction; as a result the emission measure increases and the luminosity attains maximal value $\sim 3 \times 10^{33}$ erg s $^{-1}$. This is followed by the expansion which results in the luminosity drop. At the most luminous phase, $L_x \gtrsim 10^{33}$ erg s $^{-1}$, the SN Ia remnant lives $\sim 4 \times 10^3$ yr. The temperature of the shocked ejecta at this phase is in the range of $10^8 - 10^9$ K, so only a small fraction of the total luminosity (10 – 30%) falls into the standard *Chandra* band (0.2–10 keV).

Generally, the SN expansion dynamics can be affected by the diffusion of relativistic protons into the ejecta. This process might modify dynamics by smoothing out the pressure jump at the boundary between ejecta and relativistic fluid. The time it takes to fill the SN by cosmic rays with the energy E per particle can be estimated as the time for the proton to escape from the relativistic bubble layer adjacent to SN. The volume comparable with SN of radius R is a spherical layer of a thickness of $\sim 0.3R$. Assuming Bohm diffusion coefficient $D = cr_g/3$ one gets the diffusion time

$$t_d \sim \frac{(0.3R)^2}{4D} = 1.5 \times 10^9 B_5 \left(\frac{R}{30 \text{ pc}} \right)^2 \text{ yr}, \quad (15)$$

The time it takes to fill the SN by cosmic rays at the essential deceleration epoch turns out tremendous compared to the SN age ($\sim 3 \times 10^3$ yr). We conclude, therefore, that the diffusion penetration of relativistic protons into the SN envelope unlikely affects the SN expansion dynamics.

² We use nonrelativistic equation of state in these illustrative runs even for $T_e = 10^4$ keV, although this not valid for electrons.

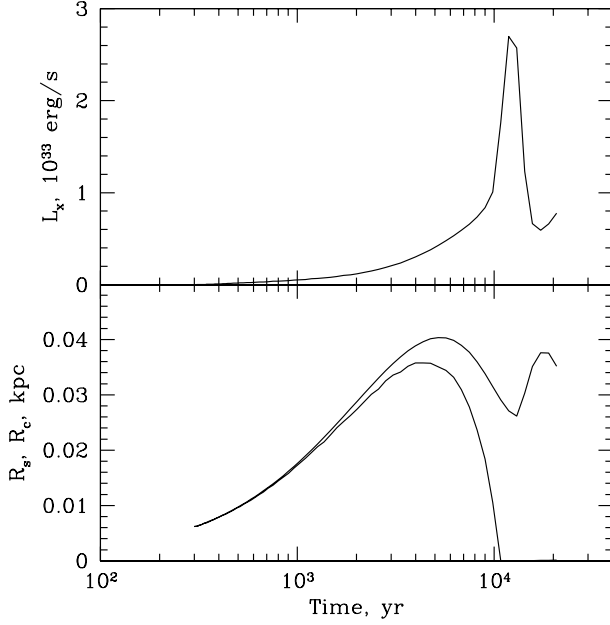


Figure 4. X-ray luminosity of the reverse shock in the model with the ICM temperature of 10^4 keV (**top**) and the radii of the contact discontinuity and reverse shock (**bottom**). The luminosity decreases after $\sim 10^4$ yr because of the significant expansion of the postshock layer between the reverse shock (**bottom**, lower curve) and the contact surface (upper curve).

3.2 SN bulk motion

After the expansion braking the SN shell still retains the bulk motion with the typical velocity $v_s = 400 \text{ km s}^{-1}$. If the deceleration of the bulk motion were negligible, the SN shell would escape the relativistic bubble after the average residence time $R_b/v_s \sim 10^7$ yr. We now check, whether the ram pressure and the Alfvén wave drag can substantially decelerate the bulk motion inside the relativistic bubble.

The ram pressure drag force exerted on the SN shell is $F_d = \pi r_{sn}^2 \rho_a v^2$, where the ambient density is $\rho_a = 3p/c^2$, assuming particles dominate in the pressure. Using the equation of motion

$$M \frac{dv}{dt} = -\pi r_{sn}^2 \rho_a v^2, \quad (16)$$

the characteristic deceleration length can be estimated as

$$l_d \approx \frac{Mc^2}{3\pi r_{sn}^2 p} \approx 69 p_{10}^{-1/3} \text{ kpc}. \quad (17)$$

This shows that the deceleration of the bulk motion of SN by the ram pressure can be neglected.

The Alfvén wave drag exerted on the spherical SN shell is defined similarly to the case of the wind shell, i.e., $F_d = (1/2)B^2(v/v_A)r_{sn}^2$. The characteristic deceleration time is $t_d \approx v_s M/F_d$, while the deceleration length, $l_d \approx v_s t_d$, is

$$l_d \approx \frac{M v_s c}{B r_{sn}^2 \sqrt{12\pi p}} \approx 0.3 v_{s,400} B_5^{-1} p_{10}^{1/6} \text{ kpc}, \quad (18)$$

where $v_{s,400} = v_s/(400 \text{ km s}^{-1})$. This shows that the Alfvén wave drag essentially brakes the bulk motion of the SN shell at the distance much smaller than the radius of the relativistic bubble even for weak field $B \sim 3 \times 10^{-6} \text{ G}$. We thus conclude that the ejecta of SN Ia exploded in the relativistic bubble cannot escape the bubble due to the bulk motion. Amazingly, the SN material is decelerated

in the slow bulk motion at the distance ten times larger than in the maximum radius attained in the high speed envelope expansion.

3.3 Rayleigh-Taylor instability and spike deceleration

The swept-up SN shell decelerating in the light relativistic fluid is liable to the Rayleigh-Taylor instability (RTI) which generally should result in the fragmentation of SN shell, close to the stage of the significant deceleration, i.e., at about the stopping radius r_{sn} . The situation is similar, albeit inverted with respect to Crab nebula. The Crab shell *accelerated* by the shocked relativistic wind shows long thin RT spikes directed backward the center (Hester et al. 1996). In case of decelerated SN dense RT spikes protruded forward could travel large distances before they stop. Yet it should be emphasised the difference with the Crab. In the latter case the SN material pressurized by the relativistic plasma is cool with the thermal velocity $u_{crab} \sim 10 \text{ km s}^{-1}$. The SN Ia material in the adiabatic reverse shock is hot with the thermal velocity $u_{sn} \sim 10^4 \text{ km s}^{-1}$. The density contrast in the Crab is therefore by factor $(u_{sn}/u_{crab})^2 \sim 10^6$ larger.

The behavior of RT spike may be affected by the KHI. For a cylinder spike of the radius a moving with the velocity v along its own axis the perturbation growth time for the most destructive wave number $k \sim 1/a$ is $t_{KH} \sim (a/v)\chi^{1/2}$, where χ is the density ratio of SN and bubble material. At the SN radius $R = 20 \text{ pc}$ the contrast $\chi \sim 10^5$. The distance at which the most dangerous mode grows is then $\sim vt_{KH} \sim a\sqrt{\chi} \sim 300a$. We do not aware of any multi-dimensional hydrodynamic simulations of a dense cloud moving in a rarefied relativistic fluid. A close analogue is the two-dimensional hydrodynamic simulations of a dense cloud moving in the post-shock intercloud rarefied gas (Klein et al. 1994). These simulations show that the cloud life time with respect to the fragmentation and fragment deceleration is order $\sim 4(a/v)\chi^{1/2}$, roughly four times larger than the Kelvin-Helmholtz time. Adopting this characteristic time one finds that the distance at which the spike will be destroyed and decelerated is $\sim 4vt_{KH} \sim 4a\chi^{1/2} \sim 10^3 a$. Assuming $a/R \sim 10^{-2}$, comparable with the fingers in case of Crab nebula (Hester et al. 1996), one finds that RT spike can travel $\sim 10R \lesssim 0.3 \text{ kpc}$, rather small distance compared to the bubble radius.

On the other hand, Nulsen (1982) argues that the increase of the width of the boundary layer due to the KHI quenches the very instability. As a result the mass loss is suppressed and eventually is defined by the momentum transfer [cf. equations (5) and (7)]. In this case the problem of mass stripping due to KHI is reduced to the problem of a deceleration of RT spikes which is analysed in the next section.

The longitudinal magnetic field also can suppress the KHI. Let ρ_1 and ρ_2 be the density of rarefied and dense fluid. According to the criterion of the KHI in the presence of magnetic field Chandrasekhar (1961) the condition that the magnetic field turns off the KHI is

$$B > (2\pi\rho_1)^{1/2}v = (6\pi p)^{1/2}\left(\frac{v}{c}\right) \approx 1.4 \times 10^{-6} \text{ G}, \quad (19)$$

where $p = 10^{-10} \text{ erg cm}^{-3}$, c is the light speed, and $v = 10^9 \text{ cm s}^{-1}$ are used. The required magnetic field $B > 1.4 \times 10^{-6} \text{ G}$ is within the range of field strength in the relativistic bubble, which can be as large as several 10^{-5} G . The magnetic stabilization of RT spikes against KHI thus seems quite plausible. Hereafter we address the deceleration of RT spike assuming its stability.

3.3.1 Drag in collisionless case

A typical RT spike is assumed to be a cylinder with the mass m , radius a , and length b , which are assumed to remain constant. The RT spike presumably moves along the axis in the relativistic plasma dominated by the relativistic particles. With the giroradius $r_g \sim 3 \times 10^{11}$ cm and the RT spike radius $a \sim 10^{-2} r_{sn} \sim 10^{18}$ cm only a motion along the regular magnetic field can be collisionless. The mean free path for relativistic protons propagating along the field can be constrained by scattering on the perpendicular component of a random field. The resulting mean free path along the mean field B is $\lambda_{\parallel} \sim r_g (B/\delta B)^2$ (Strong et al. 2007), where δB is the amplitude of a random field with resonance wave number $k_{res} r_g \sim 1$. Following Strong et al. (2007) we assume the power law spectrum of random field energy density $W(k) \propto k^{-s}$ with $s = 1.67$, between maximal length scale $k_{min} \sim 1/R_b$ and minimal scale $k_{max} \sim 1/r_g$. The integrated energy density is normalized according to suggestion by Strong et al. (2007): $W = B^2/(8\pi)$. With these prerequisites one gets $(\delta B/B)^2 \sim (k_{min}/k_{res})^{s-1} \sim 10^{-7}$ and $\lambda_{\parallel} \sim 10^7 r_g \sim 3 \times 10^{18}$ cm, i.e., $\lambda_{\parallel} \gtrsim r_g$. The situation thus is about collisionless, although uncertainties of the relevant parameters do not preclude collisional regime as well. One needs therefore to consider both collisionless and collisional cases.

For $b \gg a$ the moment exchange occurs primarily via the cosmic ray collisions with the lateral surface of the spike. The momentum transferred to the colliding particle with the energy E assuming diffusive reflection, is $\sim (E/c^2)v$. For the particle flux on the unit of surface area $(1/4)nc$, where n is the cosmic ray concentration, the moment transferred per second to all the striking protons (drag force) is $F_d = (1/2)\pi ab\epsilon(v/c)$, where $\epsilon = 3p$ is the energy density of relativistic particles. Note that the drag force could be derived also using average energy gain of a relativistic particle per collision with the cloud $E(v/c)^2$ (Fermi 1949). Indeed, for a spherical cloud the total energy loss per second in that case is $\pi a^2 nc E(v/c)^2 = \pi a^2 \epsilon v^2/c$. This implies the drag force $\pi a^2 \epsilon(v/c)$, which coincides with the above expression for F_d within the geometrical factor.

The equation of motion of the spike in the collisionless case with the above value of F_d then reads

$$m \frac{dv}{dt} = -1.5\pi ab p \frac{v}{c}. \quad (20)$$

We neglect here the head-on collisions which would contribute the term of the order $\sim a/b \ll 1$ in the right hand side. Note, the transition from spike to the spherical blob corresponds to $b = 2a$ in the drag force expression. The characteristic time of the spike deceleration is thus

$$t_d \sim \frac{2}{3} \frac{mc}{\pi ab p}. \quad (21)$$

The ratio $m/\pi a^2$ can be expressed via the surface density of the SN shell at the stopping radius as $m/\pi a^2 = \eta M/4\pi r_{sn}^2$, where the parameter $\eta \gg 1$ because the spike is formed by a shell patch with the radius $\gg a$. The deceleration distance for the spike is then

$$l_d = v t_d \sim \frac{10}{9} \eta r_{sn} \frac{c}{v} \frac{a}{b} = 1.2\eta \frac{a}{b} \text{ kpc}, \quad (22)$$

where we make use of equation (12) and adopt $v = 10^9$ cm s⁻¹ and $r_{sn} = 36$ pc. For $\eta \sim 10$ and $a/b \sim 0.1$ the spike can travel ~ 1 kpc before it gets completely decelerated. In collisionless case the RT fragments are decelerated efficiently inside the relativistic bubble. It should be stressed, however, that the collisionless regime can be realized only in the case of the motion along the magnetic

field so, only a small fraction of RT spikes experiences this type of a deceleration.

3.3.2 Drag in collisional case

If the mean free path for cosmic ray protons is small $\lambda \ll a$, one expects that the drag force should be proportional to v^2 . The general condition for that is the large Reynolds number $\text{Re} > 10^2$. To estimate Re we adopt the spike radius $a \sim 10^{-2} r_{sn} \sim 10^{18}$ cm, the spike velocity $v = 10^9$ cm, and $\lambda = r_g$ as the mean free path for relativistic protons. Assuming $B = 10^{-5}$ G, i.e., $r_g \sim 3 \times 10^{11}$ cm one gets $\text{Re} = 3av/cr_g \sim 3 \times 10^5$. The condition $\text{Re} > 10^2$ thus is fulfilled for $\lambda < 3 \times 10^4 r_g \sim 10^{15}$ cm, which is rather soft requirement.

In the collisional approximation the drag force is $F_d = 3\pi a^2 p(v/c)^2$. Following the recipe of the previous section one obtains the spike deceleration distance

$$l_d \approx \frac{5}{9} \eta r_{sn} \left(\frac{c}{v} \right)^2. \quad (23)$$

For $v = 10^9$ cm s⁻¹ and $r_{sn} = 36$ pc one obtains $l_d \sim 17\eta$ kpc, rather large value that exceeds bubble radius (5 kpc) even for modest value of $\eta \sim 1$. The ram pressure drag thus almost does not decelerate RT spikes inside the relativistic bubble.

3.3.3 Alfvén wave drag

The Alfvén wave drag can operate for the large conducting body $a > (v/c)r_g \sim 10^{10}$ cm, which is easily met for RT spikes. Using the expression for the power radiated in the form of Alfvén waves Drell et al. (1965)) one can write the Alfvén drag force acting on the plasma spike with the radius a and length b as

$$F_d = \frac{B^2}{2\pi} \frac{v}{v_A} ab, \quad (24)$$

where $v_A = B/\sqrt{4\pi\rho_a}$ is the Alfvén velocity. Note, it is only the lateral surface area ($\approx 2ab$), that matters. Following arguments of the previous sections one gets the spike deceleration distance

$$l_d \approx 5\eta r_{sn} \left(\frac{\pi}{3} \right)^{3/2} \frac{\sqrt{p}}{B} \frac{a}{b} \frac{c}{v} = 6\eta \frac{a}{b} B_5^{-1} p_{10}^{1/6} \text{ kpc}. \quad (25)$$

For fiducial model $p = 10^{-10}$ erg cm⁻³, $B = 10^{-5}$ G, $v = 10^9$ cm s⁻¹ one obtains $l_d \approx 6\eta(a/b)$ kpc. This result shows that in case $a = b$ the blob can travel the distance exceeding the radius of the relativistic bubble even for moderate values of $\eta > 2$. For a long spike ($b \gg a$) deceleration is by factor b/a stronger and the deceleration distance is accordingly shorter. For $b/a \sim 10$ and $\eta \sim 10$ the RT spike can travel ~ 6 kpc, a distance comparable with the adopted bubble radius $R_b = 5$ kpc. It takes roughly $R_b/v \sim 5 \times 10^5$ yr for the spike to reach the bubble boundary assuming the spike average velocity of 10^4 km s⁻¹.

The effect of the Alfvén wave drag is determined by the magnetic field. If the field is weak, $B = 3 \times 10^{-6}$ G, the deceleration distance is ~ 18 kpc, substantially larger than the bubble radius. On the other hand, for $B > 10^{-5}$ G the deceleration distance is smaller than the bubble radius and significant amount of RT fragments will remain in the relativistic bubble. The escape probability for RT spike in case of $B = 10^{-5}$ G can be estimated adopting mean free path $\lambda = v t_d = 6$ kpc, i.e., $\tau = R_b/\lambda = 5/6$. Equation (11) gives in this case the escape probability $p_{esc} \approx 0.6$.

[t]

Table 1. Parameters of fiducial model

Parameter	Description	Value
R_b	Bubble radius	5 kpc
t_b	Age	3×10^7 yr
p	Pressure	10^{-10} erg cm $^{-3}$
B	Magnetic field	10^{-5} G
n	Number density of ICM	0.02 cm $^{-3}$
M_s	Stellar mass in the bubble	$9 \times 10^{10} M_\odot$
\dot{N}	Stellar death rate	0.83 yr $^{-1}$
\dot{N}_{sn}	SN Ia rate	0.0066 yr $^{-1}$
r_w	Wind stopping radius	0.5 pc
r_{sn}	SN stopping radius	36 pc

3.3.4 Spike deceleration by wind material

The average number of wind shells along the average distance to the bubble boundary for the fiducial model is ~ 0.08 (Section 2.2) which means that for SN fragments the probability to collide with a wind shell is low, ~ 0.06 . A question arises, what happens, anyway, if the collision takes place.

The deceleration is determined by the ratio of column densities (μ) of the projectile (RT spike) and target (wind shell). For the wind shell

$$\mu_w = \frac{m_w}{\pi r_w^2} = 1.4 \times 10^{-4} \text{ g cm}^{-2}, \quad (26)$$

where $r_w = 1.5 \times 10^{18}$ cm and $m_w = 0.5 M_\odot$ are used. The column density of the spike $\mu_s = \eta M / (4\pi r_{sn}^2) \sim 2 \times 10^{-8} \eta \text{ g cm}^{-2} \ll \mu_w$. This comparison shows that the spike will be fully decelerated in a single collision with a wind shell. We conclude therefore that for the fiducial model there is non-negligible probability, ~ 0.06 , that the spike will be decelerated in the bubble via collision with the wind shell.

4 DISCUSSION

The aim of this paper has been to get an idea on what happens to the matter ejected by the stellar population of BCG embedded into a bubble of relativistic plasma. We have found that the expansion of a wind envelope lost by a star is stopped by the pressure of the relativistic fluid when the radius attains ~ 0.5 pc. Because of the small size of the wind shell its bulk motion is not decelerated neither by the ram pressure, nor by the Alfvén wave drag, so the shell escapes the bubble together with the parent star. The SN Ia exploding in the relativistic fluid expands up to much larger radius $\sim 30 - 40$ pc and its bulk motion can be efficiently decelerated by the Alfvén wave drag. Unless a RT instability operates, the SN material would not escape the relativistic bubble, but will instead be advected by the buoyantly rising relativistic fluid.

The RT instability can strongly modify the behavior of the ejecta. In the framework of our fiducial model we find that significant fraction of SN fragments escapes the relativistic bubble. In our analysis of this scenario we rely on the fiducial model parameters outlined in Table 1. A gas lump crossing the bubble boundary and entering the ICM is decelerated after sweeping the ICM mass comparable with its own mass. The escaping wind shell gets decelerated in the thermal plasma of ICM at the length of $l_w \sim 1$ kpc (Section 2.2). The wind deposits $\sim 1.4 \times 10^7 M_\odot$ in this layer. This value

should be compared with the mass of the ICM gas, which is already there. For $R_b = 5$ kpc and hydrogen number density $n = 0.02 \text{ cm}^{-3}$ the mass of the ICM in the boundary layer with the thickness $l_w = 1$ kpc is $7 \times 10^7 M_\odot$, i.e., factor ~ 5 larger than the mass deposited by the wind shells. The deposited wind mass scales with the bubble radius as $\propto R_b^4$, whereas the ICM mass in the layer is $\propto R_b^2$. We thus conclude that for the fiducial model the wind material escaping the relativistic bubble does not change significantly the density of the surrounding ICM; moreover the effect even smaller in case of M 87 in which bubble radius $R_b \sim 1.4$ kpc. The effect of the energy deposition by the escaping wind shells is also negligible because the bulk velocities of the wind shells is subsonic and the deposited mass is low. The chemical composition of ICM is not affected by the escaping wind shells either.

Unlike the wind shells, fragments of SN ejecta escaping the relativistic bubble may have a profound effect on the enrichment of ICM by iron peak elements. The resulting abundance is determined by the width of the mixing layer. Generally, one should consider time-dependent model of the formation of mixing layer. However, we assume that the mixing layer in the fiducial model is formed by the cumulative effect of all SNe. Employing the momentum conservation arguments a deceleration distance for the RT spike entering the ICM with the velocity v_i and decelerated down to v_f turns out to be

$$l_{sn} \sim \eta \ln(v_i/v_f) \frac{M}{4\pi r_{sn}^2 \rho} \approx 0.5 \eta \text{ pc}, \quad (27)$$

where we used $v_i/v_f = 20$, $n = 0.02 \text{ cm}^{-3}$, $M = 1.4 M_\odot$, and $r_{sn} = 36$ pc. For $\eta = 10$ one gets the deceleration length $l_{sn} \sim 5$ pc. At first glance the mixing layer could be identified with the deceleration layer. This layer contains $M_{icm} \sim 7 \times 10^5 M_\odot$ of the ICM gas. The mass produced by SN Ia during the life time of the bubble is $M_{sn} \sim 3 \times 10^5 M_\odot$. If most of the SN mass escapes the bubble, the amount of escaping iron in the mixing layer turns out to be $\sim 10^5 M_\odot$ which corresponds to the iron abundance $\sim 80 \times (\text{solar})$.

On the other hand, the mixing layer could be broader because the total volume of shocked SN fragments in pressure equilibrium substantially exceeds the volume of the deceleration layer. Simple estimate based upon the pressure equilibrium suggests the total volume occupied by shocked SN ejecta to be $V_t = N_{sn} E / p$ which implies the layer width ~ 300 pc. If this is identified with the width of the mixing layer than the iron abundance will be factor two larger compared to solar abundance of pre-existing ICM. The increase of the iron abundance by factor two changes the 0.6-2 keV emissivity³ by factors of 1.8, 1.5 and 1.3 for the gas temperatures 1, 2 and 3 keV respectively.

The latter estimates suggest complete mixing of injected iron with the ICM, which may not be the case. The point is that the deceleration of SN fragments in the ICM results in the strong heating of the ejecta material up to temperature corresponding to its kinetic energy. Most of the iron therefore ends up in the high entropy/low density gas with the very little X-ray emission. The observational outcome thus critically depends on the mixing degree between hot SN gas and the relatively cool ICM.

The above picture of mixing layer is very crude and one cannot rule out a possibility that the expanding relativistic bubble continuously catches up with the mixing layer outer boundary so that most of the decelerated SN material injected in the ICM eventually

³ 0.6-2 keV is the energy range where present day grazing incidence X-ray telescopes are most sensitive

turns out engulfed by the relativistic fluid. Qualitatively this scenario then gets similar to the case when SN Ia ejecta bulk motion is decelerated well inside the bubble. In this case no strong X-ray emission is expected from fully expanded shells (because of the very low gas density). The fate of the iron generated by SN Ia in this scenario solely depends on the evolution of relativistic plasma, which can escape the central region of the galaxy, as suggested by observations of e.g. M87 (Churazov et al. 2001; Forman et al. 2005).

5 CONCLUSIONS

We consider the outcome of the mass ejection by stars via winds and supernovae inside a bubble of relativistic plasma inflated by an AGN in the core of BCG. Wind shells are likely to escape the relativistic bubble and deposit their mass in the ICM within ~ 1 kpc from the bubble boundary. SN Ia exploded inside the bubble is efficiently decelerated owing to the pressure of the relativistic fluid. If the SN shells remain spherical until the expansion of the envelope stops and do not fragment, then they would not escape the bubble. In this case the iron produced by SN Ia is advected by the relativistic plasma and may leave the central region of the BCG together with buoyantly moving bubbles.

As a possibility we consider a scenario in which the RT instability of the SN envelope at the deceleration phase breaks the shell into multitude of RT spikes. The analysis of the deceleration of RT spikes in the relativistic fluid shows that the SN fragments are able to escape the bubble. The fragments are decelerated in the ICM in a close vicinity of the bubble boundary thus producing Fe-rich layer. In the optimistic scenario this Fe-rich layer can enhance X-ray emission around bubbles of relativistic plasma, producing bright rims around bubbles.

6 ACKNOWLEDGEMENTS

We are grateful to Nail Inogamov and Sergey Sazonov for useful discussions, and to Ewald Müller for sharing hydrocode. NC thanks Wolfgang Hillebrandt for the invitation to MPA. The work was partly supported by the Division of Physical Sciences of the RAS (the program “Extended objects in the Universe”, OFN-16) and the project NSH-5069.2010.2.

REFERENCES

Matthews J.M., Kurtz D.W., Martinez P., 1999, *ApJ*, 511, 422
 Birzan, L., Rafferty, D. A., McNamara, B. R., Wise, M. W., Nulsen, P. E. J. 2004, *ApJ*, 607, 800
 Böhringer, H., Voges, W., Fabian, A. C., Edge, A. C., Neumann, D. M. 1993, *MNRAS*, 264, L25
 Chandrasekhar, S. 1961. Hydrodynamic and hydromagnetic stability. Oxford University Press
 Churazov, E., Forman, W., Jones, C., Böhringer, H. 2000, *A&A*, 356, 788
 Churazov, E., Brügggen, M., Kaiser, C. R., Böhringer, H., Forman, W. 2001, *ApJ*, 554, 261
 Drell, S. D. Foley, S. D., Ruderman, M. A. 1965, *JGR*, 70, 3131
 Fabian, A. C., Sanders, J. S., Crawford, C. S., Conselice, C. J., Gallagher, J. S., Wyse, R. F. G. 2003, *MNRAS*, 344, 48
 Fermi, E. 1949, *PhRv*, 75, 1169

Forman, W., Nulsen, P., Heinz, S., Owen, F., Eilek, J., Vikhlinin, A., Markevitch, M., Kraft, R., Churazov, E., Jones, C. 2005, *ApJ*, 635, 894
 Forman, W., Jones, C., Churazov, E., Markevitch, M., Nulsen, P., Vikhlinin, A., Begelman, M., Böhringer, H., Eilek, J., Heinz, S., Kraft, R., Owen, F., Pahre, M. 2007, *ApJ*, 665, 1057
 Gedalin, M. 1993, *Phys. Rev. E*, 43, 4354
 Gull, S. F., Northover, K. J. E. 1973, *Nature*, 244, 80
 Hester, J. J., Stone, J. M., Scowen, P. A., et al. 1996, *ApJ*, 456, 225
 Huang, Z., Sarazin, C. 1998, *ApJ*, 496, 728
 Johnson, R., Chakrabarty, D., O’Sullivan, E., Raychaudhury, S. 2009, *ApJ*, 706, 980
 King, A. R. 1966, *AJ*, 71, 64
 Klein, R. I., McKee, C. F., Colella, P. 1994, *ApJ*, 420, 213
 Lou, Y.-Q., Zhai, X. 2010, *MNRAS*, 408, 436
 Mathews, W. G., Brighenti, F. 2003, *ApJ*, 599, 992
 McNamara, B. R. et al. 2000, *ApJL*, 534, L135
 Narayan, R., Medvedev, M. V. 2001, *ApJ*, 562, L129
 Nulsen, P. E. J. 1982, *MNRAS*, 198, 1007
 Osterbrock, D. E. 1989. Astrophysics of gaseous nebulae and active galactic nuclei. University science books, p.385
 Pritchett, C. J., Howell, D. A., Sullivan, M. 2008, *ApJL*, 683, L25
 Richer, M. G., Lopez, J. A., Pereyra, M., Riesgo, H., Garcia-Diaz, M. T., & Baez, S.-H. 2008, *ApJ*, 689, 203
 Salaris, M., Serenelli, A., Weiss, A., Miller Bertolami, M. 2009, *ApJ*, 692, 1013
 Sanders J. S., Fabian A. C., Heating versus Cooling in Galaxies and Clusters of Galaxies, ESO Astrophysics Symposia, Springer-Verlag Berlin Heidelberg, 2007, 74
 Schaller, G., Schaerer, D., Meynet, G., Maeder, A. 1992, *A&AS*, 96, 269
 Stage, M. D., Allen, G. E., Houck, J. C., Davis, J.E. 2006, *Nature Phys.*, 2, 614
 Steffen, M., Szczerba, R., Schoenberner, D. 1998, *A&A*, 337, 149
 Strong, A. W., Moskalenko, I. V., Ptuskin, V. S. 2007, *ARNPS*, 57, 285
 Vassiliadis, E., Wood, P. R. 1993, *ApJ*, 413, 641
 Wu, X., Tremaine, S. 2006, *ApJ*, 643, 210